15. Nugent, J. M. & Palmer, J. D. in *Plant Mitochondria* (eds Brennicke, A. & Kück, U.), 163–170 (VCH, Weinheim, 1993).
16. Wolfe, K. H., Li, W.-H. & Sharp, P. M. Rates of nucleotide substitution vary greatly among plant mitochondrial, chloroplast, and nuclear DNAs. *Proc. Natl Acad. Sci. USA* **84,** 9054–9058 (1987).
17. Palmer, J. D. & Herbon, L. A. Plant mitochondrial DNA evolves rapidly in structure, but slowly in sequence. *J. Mol. Evol.* **28,** 87–97 (1988).
18. Samigullin, T. H. *et al.* Sequences of rDNA internal transcribed spacers from the chloroplast DNA of 26 bryophytes: properties and phylogenetic utilities. *FEBS Lett.* **422,** 47–51 (1998).
19. Sluiman, H. J. A cladistic evaluation of the lower and higher green plants. *Plant Syst. Evol.* **149,** 217–232 (1985).
20. Doyle, J. J. & Doyle, J. S. A rapid DNA isolation procedure for small quantities of fresh leaf tissue. *Phytochem. Bull.* **19,** 11–15 (1987).
21. Doyle, J. A. & Donoghue, M. J. Seed plant phylogeny and the origin of angiosperms: an experimental cladistic approach. *Bot. Rev.* **52,** 321–431 (1986).
22. Pryer, K. M., Smith, A. R. & Skog, J. E. Phylogenetic relationships of extant ferns based on evidence from morphology and *rbcL* sequences. *Am. Fern J.* **85,** 205–282 (1995).
23. Chaw, S.-M., Zharkikh, A., Sung, H.-M., Lau, T.-C. & Li, W.-H. Molecular phylogeny of extant gymnosperms and seed plant evolution: analysis of nuclear 18S rRNA sequences. *Mol. Biol. Evol.* **14,** 56–68 (1997).

Acknowledgements. We thank K. Adams, G. J. Gastony and P. Kuhlman for critical reading of the manuscript, R. C. Brown, B. Crandall-Stotler, G. J. Gastony, B. D. Mishler, K. S. Renzaglia, J. Shaw, H. J. Sluiman, A. R. Smith, S. H. Strauss, D. Waters and J. A. Wheeler for plant material, F. Dong and K. G. Wilson for probes, and G. Burger, M. W. Gray, B. F. Lang, C. Lemieux and M. Turmel for unpublished data. This work was supported by grants to Y.Q. and J.D.P. from the NIH.

Correspondence and requests for materials should be addressed to J.D.P. (e-mail: jpalmer@bio.indiana.edu).

Noise and determinism in synchronized sheep dynamics

B. T. Grenfell*, K. Wilson†, B. F. Finkenstädt*, T. N. Coulson‡, S. Murray§, S. D. Albon‖, J. M. Pemberton¶, T. H. Clutton-Brock* & M. J. Crawley#

** Zoology Department, University of Cambridge, Downing Street, Cambridge CB2 3EJ, UK*
† Department of Biological and Molecular Sciences, University of Stirling, Stirling FK9 4LA, UK
‡ Institute of Zoology, Zoological Society of London, Regent's Park, London NW1 4RY, UK
§ Scottish Natural Heritage, Clachcaran, Stilligarry, South Uist, Western Isles HS8 5RS, UK
‖ Institute of Terrestrial Ecology, Hill of Brathens, Glassel, Banchory AB31 4BY, UK
¶ Institute of Cell, Animal and Population Biology, University of Edinburgh, West Mains Road, Edinburgh EH9 3JT, UK
 # Imperial College, Silwood Park, Ascot SL5 7PY, UK

A major debate in ecology concerns the relative importance of intrinsic factors and extrinsic environmental variations in determining population size fluctuations[1–6]. Spatial correlation of fluctuations in different populations caused by synchronous environmental shocks[2,7,8] is a powerful tool for quantifying the impact of environmental variations on population dynamics[8,9]. However, interpretation of synchrony is often complicated by migration between populations[8,10]. Here we address this issue by using time series from sheep populations on two islands in the St Kilda archipelago[11–13]. Fluctuations in the sizes of the two populations are remarkably synchronized over a 40-year period. A nonlinear time-series model shows that a high and frequent degree of environmental correlation is required to achieve this level of synchrony. The model indicates that if there were less environmental correlation, population dynamics would be much less synchronous than is observed. This is because of a threshold effect that is dependent on population size; the threshold magnifies random differences between populations. A refined model shows that part of the required environmental synchronicity can be accounted for by large-scale weather variations. These results underline the importance of understanding the interaction between intrinsic and extrinsic influences on population dynamics[14].

Much ecological debate has focused on the interaction between noise and nonlinear dynamics in generating population cycles[5,6,13,15–18] and patterns of spatial synchrony[8,10,19]. Here we use the unusual circumstance of long parallel time series from close—but completely isolated—populations as a tool with which to explore these issues.

Feral sheep populations on islands in the St Kilda archipelago have been monitored since 1955 (ref. 11) (Fig. 1). The most detailed series comprise continuous annual records for Soay sheep on the main island, Hirta, and 18 years of counts for Blackface sheep on Boreray; the islands are 3.5 km apart.

Both series show irregular population fluctuations, reflecting repeated mass mortalities of sheep[12,20] (Fig. 1a). Counts of sheep on the two islands are highly correlated (Fig. 1b) for the logged series. Pearson's $r = 0.685$ (95% bootstrap confidence limits are 0.447–0.838). As the two populations are completely separate, this synchrony indicates a high correlation in extrinsic environmental

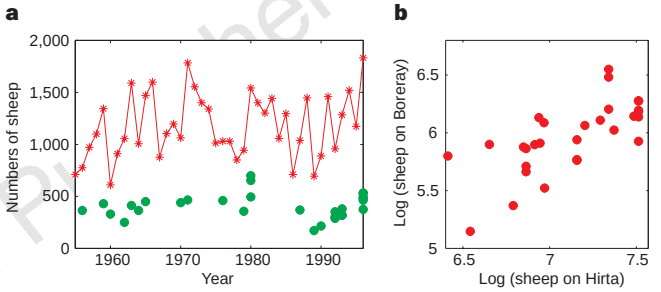

Figure 1 Feral sheep populations on Hirta and Boreray. **a**, Time series of total sheep counts from Hirta (red)[10,19] and Boreray (green). Boreray counts were obtained either on the island itself or from a circumnavigating boat. Both methods allow most of the island to be observed and produce similar figures. The Boreray counts are replicated in some years, showing that the estimates are consistent. **b**, Scatter plot of the two island time series (logged). To allow easy comparison with the models, we calculated the correlation coefficient after replacing replicate Boreray counts for a given year with their maximum.

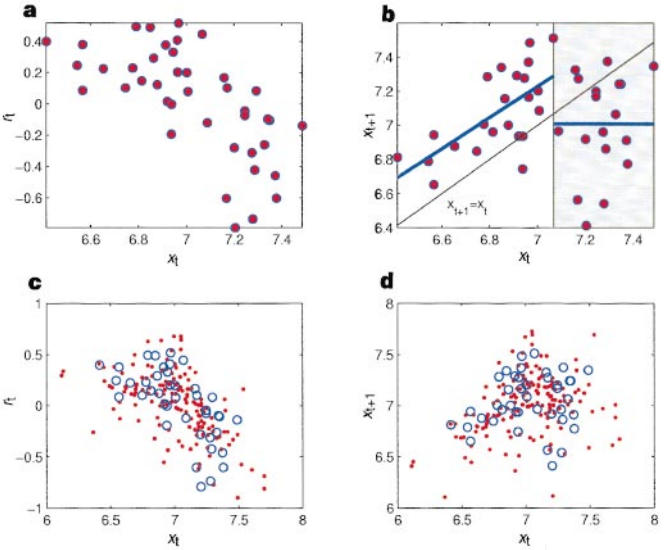

Figure 2 Modelling the Hirta time series. **a**, Plot of annual population growth rate, $r_t = x_{t+1} - x_t$, against log population size, x_t. **b**, Fit of univariate SETAR model (see Table 1a) to the scatter plot of x_{t+1} against x_t. The shaded area shows the regime above the population threshold, $x_t = C = 7.066$; blue lines show the best-fit model; and the diagonal black line is at $x_{t+1} = x_t$. **c**, A comparison of the observed r_t versus x_t plot (blue, open circles) with 150 iterates of the best-fit model with added noise (red dots), as defined in Table 1; a transient of 250 years was run off before recording the points. **d**, The same comparison as that shown in **c**, but plotted as x_{t+1} against x_t.

Table 1 Fits of threshold autoregressive models to the Hirta Soay sheep time series

	Estimate	Standard error	t	P
a Basic threshold model				
Regime 0: below-fit threshold, $C = 7.066$				
a_0	0.848	1.564	0.542	0.3*
b_0	0.912	0.229†	3.98	$<10^{-5}$*
σ_0	0.183			
Regime 1: above threshold				
A_1	7.01	0.069	101	$<10^{-5}$
b_1	0	–	–	–
σ_1	0.293			
b Threshold model with weather covariates				
Regime 0: below best-fit threshold, $C = 7.17$				
a_0	0.0217	1.66	0.013	0.495
b_0	0.811	0.209	3.883	0.0005
c_0	–0.0073	0.0004	–1.769	0.05
d_0	0.214	0.052	4.08	0.0003
σ_0	0.149			
Regime 1: above threshold				
a_1	7.174	0.0955	75	$<10^{-5}$
b_1	0	–	–	–
c_1	–0.00157	0.0007	–2.208	0.024
d_1	0	–	–	
σ_1	0.246			

Parameter estimates and associated significance levels are shown for the best-fit models; a zero coefficient indicates that the relevant term is not significant enough to be included. **a**, Estimates for the model without weather covariates (equation (1)). **b**, The model with weather covariates (equation (2)). We included two significant weather variables g, the number of hours of March gales, and h, the mean April temperature (precipitation did not account for any significant variation).
* Probabilities are only approximate levels of significant differences from zero; the AIC is the criterion used for establishing the minimal model.
† b_0 is not significantly different from 1.

influences on population fluctuations[7]. We studied the causes of population synchronization using a simple model for the relative influence on sheep population dynamics of forces dependent on extrinsic noise and intrinsic density.

We analysed the data as log (population numbers), $x_t = \log(N_t)$ (see Methods). Figure 2a shows the basic pattern of density dependence in the Hirta population by a standard plot of log (population growth rate), $r_t = x_{t+1} - x_t$, against log (population numbers), x_t (ref. 2). The figure shows that growth rate declines as population size increases, as a result of intraspecific competition for food[11,20]. There is also marked variation around this trend and the variance is greater at high population density.

The general approach to modelling this interaction between noise and density dependence is to express x_{t+1} as a function (f) of previous population sizes, as follows: $x_{t+1} = f(x_t, x_{t-1}, x_{t-2}, \ldots) + \epsilon_{t+1}$ (refs 21–23), where ϵ represents the additive variation around the relationship. In some cases, f reflects a nonlinear relationship between current and past population sizes[23]. To allow for this possibility, we fit a nonlinear self-exciting threshold autoregressive (SETAR) model[23–25] to the Hirta time series. This method approaches the problem of nonlinearity in time-series models by estimating the optimal piecewise linear model for the function f (Table 1 and Fig. 2b).

The analysis (Table 1a) shows that only time lags of up to one year account for sufficient variation to be included in the model. The best-fit model

$$\begin{aligned} x_{t+1} &= a_0 + b_0 x_t + \epsilon_{0,t+1} \quad & x_t \leqslant C \\ x_{t+1} &= a_1 + \epsilon_{1,t+1} & x_t > C \end{aligned} \tag{1}$$

displays evidence of nonlinearity, captured by a change in dynamics at a population threshold, C ($\exp(C) = 1,172$ individuals); this is seen in the plot of x_{t+1} against x_t (Fig. 2b). Below C, the dynamics follow a simple recurrence relationship between x_{t+1} and x_t, modified by additive normally distributed noise ($\epsilon_{0,t+1} \sim N(0, \sigma_0^2)$). The intercept, a_0, controls the mean density-independent population growth rate. The estimated slope, b_0, is not significantly different from unity (Table 1a), indicating that there is no evidence of density-dependent constraints on population growth at low numbers[21]. In contrast, above the threshold, x_{t+1} is independent of x_t and highly variable (Fig. 2b).

The model shows that there is a noisy exponential increase in population size when numbers are low following a population crash. At high densities, the population can increase, remain constant or fall, depending on environmental conditions. Simulation of the model with noise captures the essential features of both the growth-rate pattern (Fig. 2c) and the map of x_{t+1} versus x_t (Fig. 2d).

What does this analysis tell us about the high level of observed correlation between the Hirta and Boreray populations? Assuming that the Hirta model applies to both islands, we can use it to estimate the level of correlation in environmental noise required to generate the observed synchrony in population fluctuations. Specifically, we assessed how the nonlinear change in dynamics across the population threshold, C, affects the relationship between environmental correlation and population synchrony. An appropriate null model is provided by the Moran effect[7], which applies to the synchrony of isolated populations described by a common linear autoregressive regime. Moran's theorem[2] states that the asymptotic correlation of populations following identical linear autoregressive models will equal the correlation between random environmental perturbations. In a single regime with no threshold, the expected environmental correlation would therefore equal the observed correlation between populations, $r = 0.685$, as shown in Fig. 3.

In fact, Fig. 3a shows that much higher levels of noise correlation ($r > 0.9$, on average) are needed to generate the observed correlation between sheep populations on the two islands. This is because of the density-dependent nonlinearity in the system[2], which we capture by the threshold. Fluctuations both above and below the

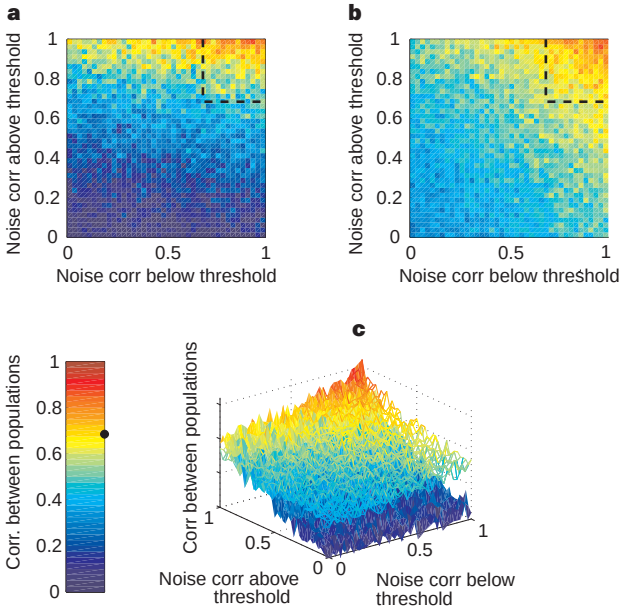

Figure 3 Simulations of the observed correlation in sheep counts between islands. Results are shown as contour maps of population correlation, as a function of inter-island correlation in environmental noise below and above the population threshold. Population correlation is colour coded as shown in the colour key, which marks the observed population correlation ($r = 0.685$) as a black dot. **a**, Correlations from the basic SETAR model, equation (1); the dashed lines show the expected environmental correlation ($r = 0.685$) required to explain the island synchrony, based on Moran's theorem. **b**, Correlation contours, as in **a**, but using the model with added weather covariates (equation (2)). **c**, Island correlations for the weather covariate model, as in **b**, but plotted as a (transparent) surface. The equivalent surface for the basic SETAR model (**a**) is shown as the underlying solid surface.

threshold need to be highly synchronized to generate the observed population correlation. The asymmetry of Fig. 3a also indicates that environmental synchrony above the threshold is the more powerful correlating force.

The correlation analysis shows that the populations are influenced by frequent extrinsic environmental variations at all population levels. We studied underlying mechanisms by including observed large-scale meteorological covariates (monthly wind, rain and temperature) in the model (see Table 1b). The best-fit model:

$$\begin{aligned} x_{t+1} &= a_0 + b_0 x_t + c_0 g_{t+1} + d_0 h_{t+1} + \epsilon_{0,t+1} \quad x_t \leqslant C \\ x_{t+1} &= a_1 + c_1 g_{t+1} + \epsilon_{1,t+1} \quad x_t > C \end{aligned} \tag{2}$$

has the same basic structure as equation (1), but now includes two extra terms. First, it includes a negative effect of March gales (hours of gales, g_{t+1}) on population growth rate, both above and below the threshold: gales are likely to increase the death rate of sheep, which are at their lowest physiological ebb at this time[20]. Second, a positive effect of April temperature, h_{t+1}, on population growth rate below the threshold is included; presumably temperature affects the timing of rapid grass growth. The parameters c_0, c_1 and d_0, d_1 control the strength of gale and temperature effects, respectively

The new model allows us to assess how synchrony in weather affects the inter-island population correlation. We assume that the gales and temperature are the same for the two islands. How much 'extra' correlation do we need in the remaining unexplained variability above and below the threshold to generate the observed level of population correlation? To determine this, we repeated the correlation analysis of Fig. 3a using the model with added weather covariates (Fig. 3b, c). The inclusion of common weather effects can account for part of the inter-island population correlation—the 'unexplained' residual environmental correlation required to the population synchrony is reduced from >0.9 to around 0.7 (Fig. 3b). The common weather pattern generates an inter-island population correlation of about 0.3 when the unexplained residual noise is uncorrelated (that is, at the three-dimensional origin of Fig. 3c).

This analysis underlines that the observed inter-island population synchrony is remarkably high. We required an average environmental correlation of over 0.9—well above the prediction of the Moran effect—to achieve the observed population correlation of ~0.7. This is because of the density-dependent nonlinearity in the system[2]. Specifically, the two sheep populations must both be sufficiently entrained by the same environmental conditions to cross the population threshold, C, in the same year if they are to remain highly synchronized. This result has general implications for the application of models for environmental entrainment of spatial dynamics[8,10,19] to systems that exhibit threshold behaviour.

Analysis of the inter-island correlation also provides a powerful tool for dissecting the internal dynamics of the populations. First, the SETAR model (equation (1)) extends the conclusions of previous studies of the Hirta population[13,20]. There is a threshold sheep density that is determined by food availability; above this density the population can undergo spectacular crashes, which are consistent with strong, and sharply focused, overcompensatory density dependence[13]. However, populations above the threshold need not necessarily crash. At high population density, even though the average density-independent growth rate is negative (Fig. 2a), the variance in population growth rate is high enough that the population size can sometimes increase. Essentially the same dynamical pattern is apparent in the Boreray series.

Second, the inclusion of meteorological covarites in the model explains part of the interaction between density-dependent and -independent forces. The population takes two years after a population crash to rise again to high levels[20]. If this rise above the threshold coincides with severe spring gales, they increase the chance of another severe crash. The probability and degree of overcompensatory density dependence therefore depend on the weather.

Finally, the portion of inter-island correlation that remains unexplained by the available weather covariates (Fig. 3d) shows that there is a good deal more to understand about the dynamics of crashes in mechanistic terms. Specifically, it seems likely that some combination of food shortage[12], parasitism[26,27] and the timing of bad weather stresses the sheep enough to precipitate crashes. In high-density years, the system appears to be exquisitely sensitive to this combination of density-dependent and -independent factors.

Our results underline the importance of detailed long-term studies for teasing out the interaction of deterministic and stochastic influences on population fluctuations[14]. Threshold models with meteorological covariates[24] provide a useful method with which to analyse these issues. □

Methods

Fitting the threshold autoregressive models. This general approach to modelling nonlinearity in time series[24] partitions the process into regimes that follow linear autoregressive models. Estimation is relatively straightforward, as the linear theory applies to the subregimes[25]. The method is particularly useful for the sheep series as it allows, first, for changes in noise variance with population size (by permitting different noise levels for each regime) and, second, the straightforward addition of weather covariates (Table 1). We based the model on log (population number), as this allows naturally for the possibility of density dependence within each regime, as indicated by a previous model of the system[13], which showed threshold-like behaviour for the 1985–91 data. In fact, a threshold model based on absolute population abundance (N_t) generates similar qualitative results to the models used here.

An important issue in model selection is the order (maximum number of lags) in each regime. We estimated this up to a lag of five years, by minimizing the Akaike information criterion (AIC)[24,28]. We also used the AIC to identify the best-fit threshold model, allowing for degrees of freedom. The best-fit SETAR model is of order 1, with five parameters (AIC = −109.97, compared to −107.57 for the best linear autoregressive (0) model with one parameter). The fit indicates a significant discontinuity in the observed dynamics across the threshold (captured by the break in the blue lines in Fig. 2b). Forcing a continuous unimodal deterministic skeleton (either a broken line model, or a low-order polynomial) gives qualitatively the same island correlation results as those shown in Fig. 3. However, such models (not shown) do not capture the observed threshold in both noise and determinism as well as does equation (1).

Weather covariates. We tested a range of weather variables for inclusion in the model. On Hirta most mortality occurs at the end of winter in March and April when many animals can die of starvation[11,12]. Research on other breeds of sheep has shown that extreme weather conditions at times close to lambing can cause perinatal mortality[29] and that poor weather can decrease the proportion of time an individual spends feeding[30]. Consequently we considered mean monthly temperature, mean monthly precipitation and the total number of hours with wind speeds of over 34 knots during the months of March and April as possible causes of the observed correlations between islands. Weather data were provided by the UK Meteorological Office and come from the closest meteorological station, on the island of Benbecula (Outer Hebrides), 80 km east of St Kilda.

Simulations of the island correlation. We calculated each point in the 40×40 contour maps (Fig. 3) from replicate pairs of simulations of the specified model. The second simulation had a different series of random shocks from the first, adjusted to give the correlation between the two noise series above and below the threshold, C, specified by the axes of the plot. Correlations between the (logged) series were calculated for 800 years, after a transient of 250 years. We calculated the simulated weather covariates shown in Fig. 3c by bootstrapping (resampling with replacement) the observed series, to generate long, simulated time series of March gales and April temperatures. We sampled the weather data as annual (gale, temperature) pairs.

Received 10 October 1997; accepted 2 June 1998.

1. May, R. M. *Stability and Complexity in Model Ecosystems* (Princeton University Press, NJ, 1973).
2. Royama, T. *Analytical Population Dynamics* (Chapman and Hall, London, 1992).
3. Stenseth, N. C., Bjornstad, O. N. & Saitoh, T. A gradient from stable to cyclic populations of *Clethrionomys rufocanus* in Hokkaido, Japan. *Proc. R. Soc. Lond. B* **263,** 1117–1126 (1996).
4. Sugihara, G. Ecology—from out of the blue. *Nature* **378,** 559–560 (1995).

5. Ellner, S. & Turchin, P. Chaos in a noisy world—new methods and evidence from time-series analysis. *Am. Nat.* **145,** 343–375 (1995).
6. Leirs, H. *et al.* Stochastic seasonality and nonlinear density-dependent factors regulate population size in an African rodent. *Nature* **389,** 176–180 (1997).
7. Moran, P. A. P. The statistical analysis of the Canadian lynx cycle: II syhchronisation and meteorology. *Aust. J. Zool.* **1,** 291–298 (1953).
8. Ranta, E., Kaitala, V., Lindstrom, J. & Helle, E. The Moran effect and synchrony in population dynamics. *Oikos* **78,** 136–142 (1997).
9. Hill, J. K., Thomas, C. D. & Lewis, O. T. Effects of habitat patch size and isolation on dispersal by *Hesperia* comma butterflies: implications for metapopulation structure. *J. Anim. Ecol.* **65,** 725–735 (1996).
10. Bjornstad, O. N., Falck, W. & Stenseth, N. C. Geographic gradient in small rodent density-fluctuations—a statistical modeling approach. *Proc. R. Soc. Lond. B* **262,** 127–133 (1995).
11. Jewell, P. A., Milner, C. & Morton-Boyd, J. *Island Survivors* (Athlone, London, 1974).
12. Clutton-Brock, T. H., Price, O. F., Albon, S. D. & Jewell, P. A. Persistent instability and population regulation in Soay sheep. *J. Anim. Ecol.* **60,** 593–608 (1991).
13. Grenfell, B. T., Price, O. F., Albon, S. D. & Clutton-Brock, T. H. Overcompensation and population cycles in an ungulate. *Nature* **355,** 823–826 (1992).
14. Sugihara, G. Red/blue chaotic power spectra. *Nature* **381,** 199–199 (1996).
15. Grenfell, B. T. Chance and chaos in measles dynamics. *J. R. Stat. Soc. B* **54,** 383–398 (1992).
16. Falck, W., Bjornstad, O. N. & Stenseth, N. C. Voles and lemmings—chaos and uncertainty in fluctuating populations. *Proc. R. Soc. Lond. B* **262,** 363–370 (1995).
17. Stenseth, N. C. Snowshoe hare populations—squeezed from below and above. *Science* **269,** 1061–1062 (1995).
18. Higgins, K., Hastings, A., Sarvela, J. N. & Botsford, L. W. Stochastic dynamics and deterministic skeletons: population behavior of Dungeness crab. *Science* **276,** 1431–1435 (1997).
19. Ranta, E., Kaitala, V., Lindstrom, J. & Linden, H. Synchrony in population dynamics. *Proc. R. Soc. Lond. B* **262,** 113–118 (1995).
20. Clutton-Brock, T. H. *et al.* Stability and instability in ungulate populations: an empirical analysis. *Am. Nat.* **149,** 195–219 (1997).
21. Hassell, M. P., Lawton, J. H. & May, R. M. Patterns of dynamical behaviour in single-species populations. *J. Anim. Ecol.* **45,** 471–486 (1976).
22. Turchin, P. Nonlinear time-series modeling of vole population fluctuations. *Res. Pop. Ecol.* **38,** 121–132 (1996).
23. Stenseth, N. C., Falck, W., Bjornstad, O. N. & Krebs, C. J. Population regulation in snowshoe hare and Canadian lynx: asymmetric food web configurations between hare and lynx. *Proc. Natl Acad. Sci. USA* **94,** 5147–5152 (1997).
24. Tong, H. *Non-linear Time Series: a Dynamical Systems Approach* (Oxford Univ. Press, 1990).
25. Tsay, R. S. Testing and modelling threshold autoregressive processes. *J. Am. Stat. Assoc.* **84,** 230–240 (1989).
26. Gulland, F. M. D. Role of nematode infections in mortality of Soay sheep during a population crash on St Kilda. *Parasitology* **105,** 493–503 (1992).
27. Grenfell, B. T., Wilson, K., Isham, V. S., Boyd, H. E. G. & Dietz, K. Modelling patterns of parasite aggregation in natural populations: trichostrongylid nematode-ruminant interactions as a case study. *Parasitology* **111,** S135–S151 (1995).
28. Framstad, E., Stenseth, N. C., Bjornstad, O. N. & Falck, W. Limit cycles in Norwegian lemmings: tensions between phase-dependence and density-dependence. *Proc. R. Soc. Lond. B* **264,** 31–38 (1997).
29. Cloete, S. W. P., Van Halderen, A. & Schneider, D. J. Causes of perinatal lamb mortality amongst dormer and SA mutton Merino lambs. *J. S. Afr. Vet. Assoc.* **64,** 121–125 (1993).
30. Champion, R. A., Rutter, S. M., Penning, P. D. & Rook, A. J. Temporal variation in grazing behavior of sheep and the reliability of sampling periods. *Appl. Anim. Behav. Sci.* **42,** 99–108 (1994).

Acknowledgements. We thank Scottish Natural Heritage and the National Trust for Scotland for permission to work on St Kilda, and their staff for assistance, support and encouragement; J. M. Pilkington, A. McColl, A. Robertson and I.R. Stevenson for help with the project; P. Rohani for comments on the manuscript; H. Tong for statistical advice and encouragement; and the Royal Artillery for logistical support on St Kilda. The work was funded by grants from the Natural Environment Research Council (to T.H.C.-B., M.J.C., B.T.G., K.W. and S.D.A.), the Royal Society (to M.J.C., K.W. and S.D.A.) and the Biotechnology and Biological Sciences Research Council (to J.M.P.).

Correspondence and requests for materials should be addressed to B.T.G. (e-mail: bryan@zoo.cam.ac.uk).

Cortical area MT and the perception of stereoscopic depth

Gregory C. DeAngelis*, Bruce G. Cumming† & William T. Newsome*

* *Howard Hughes Medical Institute and Department of Neurobiology, Stanford University School of Medicine, Stanford, California 94305, USA*
† *University Laboratory of Physiology, Parks Road, Oxford OX1 3PT, UK*

Stereopsis is the perception of depth based on small positional differences between images formed on the two retinae (known as binocular disparity). Neurons that respond selectively to binocular disparity were first described three decades ago[1,2], and have since been observed in many visual areas of the primate brain, including V1, V2, V3, MT and MST[3–8]. Although disparity-selective neurons are thought to form the neural substrate for stereopsis, the mere existence of disparity-selective neurons does not guarantee that they contribute to stereoscopic depth perception. Some disparity-selective neurons may play other roles, such as guiding vergence eye movements[9,10]. Thus, the roles of different visual areas in stereopsis remain poorly defined. Here we show that visual area MT is important in stereoscopic vision: electrical stimulation of clusters of disparity-selective MT neurons can bias perceptual judgements of depth, and the bias is predictable from the disparity preference of neurons at the stimulation site. These

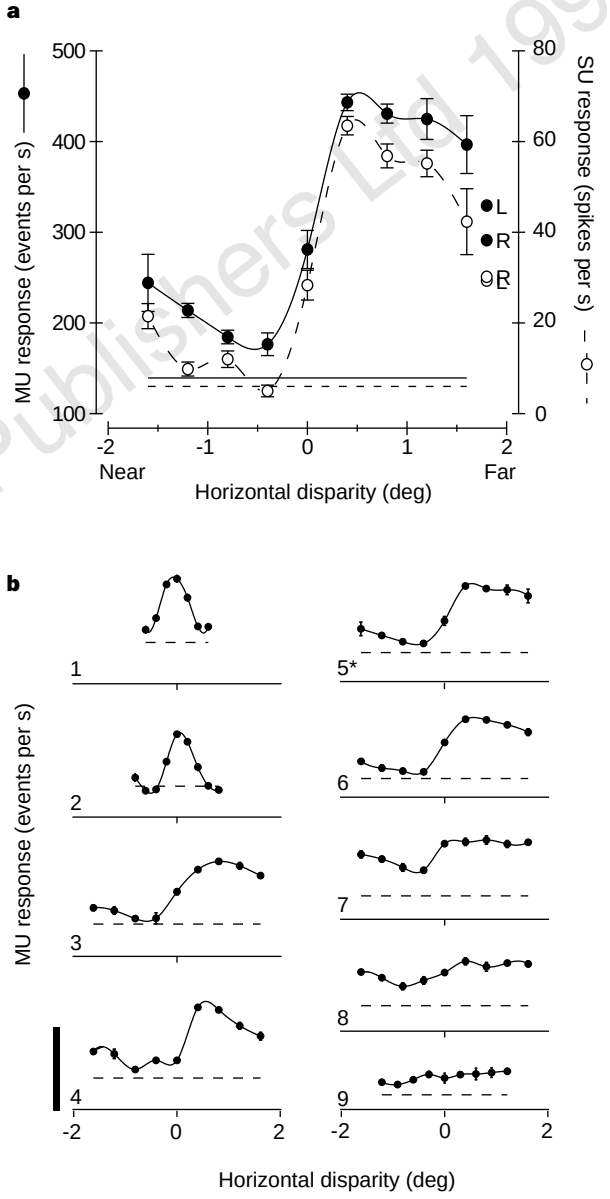

Figure 1 MT neurons are clustered according to disparity selectivity. **a**, Filled circles show multiunit (MU) responses to a drifting random-dot pattern; each datum is the mean of four responses ±1 s.e. The solid curve is a cubic spline interpolation. Filled circles labelled 'L' and 'R' denote multiunit responses to the same visual stimulus presented monocularly to either the left or the right eye, respectively. The solid horizontal line gives the multiunit response in the absence of a visual stimulus (spontaneous activity). Open circles and the dashed curve show responses of an isolated single unit (SU) recorded simultaneously. The dashed horizontal line gives the spontaneous activity level of the single unit. **b**, Sequence of disparity-tuning curves recorded at 100 μm intervals along an electrode penetration through MT in monkey S. Standard error bars are generally hidden by the data points. Curves are cubic spline interpolations, and dashed lines represent the spontaneous activity level. Height of scale bar is 400 events per second. Multiunit responses from site 5 (marked by an asterisk) are the same data shown in **a**.